ISSN 1330-3651 (Print), ISSN 1848-6339 (Online)
Received: 16 August 2025; Accepted: 17 December 2025

https://doi.org/10.17559/TV-20250816002905
Original scientific paper

Cassegrain Antenna Assisted LTE Waveform Transmission over SDR for Robust RF Based Remote Sensing Applications

Indira S.*, Jayanthi K. B.

Abstract: Remote sensing has become a critical technology for applications in earth observation, environmental monitoring, defence surveillance, and disaster management. Traditional systems often depend on optical or Synthetic Aperture Radar (SAR) sensors, which can be constrained by atmospheric conditions, high costs, or limited adaptability in dynamic environments. To overcome these challenges, this research introduces a novel Cassegrain antenna–assisted remote sensing system utilizing Long-Term Evolution (LTE) waveforms transmitted and received through Software-Defined Radio (SDR) platforms. The Cassegrain antenna, with its high directional gain, low sidelobe levels, and compact design, enhances long-range signal reception and spatial resolution, making it well suited for large-area monitoring. In parallel, LTE waveforms provide a cost-effective and readily available probing signal, enabling passive remote sensing without requiring dedicated radar infrastructure. The integration of SDR platforms further ensures flexibility, real-time adaptability, and reconfigurability of the system, allowing seamless experimentation across different spectrum bands and operational conditions. The proposed framework transforms the received LTE-based signals into spectrogram representations, from which robust spectral and temporal features are extracted. To ensure reliability under diverse conditions, a Scale-Invariant Deep Feature Learning Module (SIDFLM) is introduced, enabling consistent signal characterization despite variations in scale, orientation, or environmental interference. Experimental evaluations validate that the Cassegrain-LTE-SDR system significantly improves signal robustness, sensitivity, and scalability compared to conventional antenna-waveform configurations. Overall, this research demonstrates that combining high-gain Cassegrain antennas with LTE waveform-based SDR systems provides a reliable, efficient, and adaptable solution for next-generation RF-based remote sensing, with impactful applications in defence, agriculture, and disaster monitoring.

Keywords: cassegrain antenna; LTE waveform; remote sensing; RF signal processing; software-defined radio (SDR)

1 INTRODUCTION

Remote sensing systems are increasingly reliant on robust, adaptive, and intelligent RF communication frameworks to meet the demands of dynamic environments and mission-critical applications. Traditional sensing architectures often struggle with scalability, signal degradation, and classification accuracy under varying operational conditions. To address these challenges, we propose a novel framework that integrates Cassegrain antenna-assisted LTE waveform transmission over SDR with a Scale-Invariant Deep Features Learning-based Bagging Ensemble Classifier (SIDFL-BEC).

The use of Cassegrain antennas enables high-gain, narrow-beam RF transmission, enhancing spatial resolution and minimizing interference in long-range sensing scenarios. By leveraging LTE waveforms for their spectral efficiency and resilience transmitted via SDR platforms, the system achieves flexible, real-time modulation and adaptive control across diverse frequency bands. This configuration supports robust RF-based remote sensing, particularly in environments where signal integrity and directional precision are paramount [1-3].

To further strengthen the system's analytical capabilities, we introduce SIDFL-BEC, a hybrid deep learning model designed to extract scale-invariant features from received RF signals and classify them with high accuracy. The ensemble classifier employs bagging techniques to mitigate overfitting and enhance generalization, making it well-suited for noisy or heterogeneous data conditions. Together, these components form a scalable and intelligent sensing architecture capable of operating in complex, real-world scenarios such as environmental monitoring, disaster response, and secure surveillance [3-6].

Unlike conventional SDR-based remote sensing systems that primarily rely on static waveform configurations and shallow feature extraction techniques, the proposed framework introduces a dynamic, Cassegrain antenna-assisted LTE waveform transmission architecture integrated with a Scale-Invariant Deep Features Learning-based Bagging Ensemble Classifier (SIDFL-BEC). This hybrid approach not only leverages the directional precision and high gain of Cassegrain antennas for enhanced signal fidelity, but also utilizes LTE waveforms for standardized, adaptive RF communication over SDR platforms. The SIDFL-BEC model further distinguishes the system by enabling robust classification of RF signatures under scale variations and environmental noise, outperforming traditional single-model classifiers. This synergy of hardware adaptability and intelligent signal interpretation marks a significant advancement in scalable, resilient, and intelligent RF-based remote sensing.

2 LITERATURE SURVEY

Recent work in electrical discharge machining (EDM) of Ti-6Al-4V alloy introduced a multiphase optimization technique that achieved a 58% increase in material removal rate (MRR) and a 62.48% reduction in tool wear rate (TWR) compared to baseline settings [7]. Machine learning (ML) and deep learning (DL) have accelerated antenna design across domains such as millimeter-wave, body-centric, satellite, UAV, and textile antennas, reducing simulation overhead and enhancing computational efficiency [8].

Nature-inspired optimization using variable-resolution electromagnetic (EM) frameworks allows population-based algorithms like particle swarm optimization to begin with coarse simulations and adapt fidelity dynamically [9]. Comparative studies of 28 GHz patch antennas using Rogers RT5880 and FR-4 substrates revealed significant performance differences, with Rogers achieving 89.66% efficiency and 7.63 dBi gain versus FR-4's 52.65% efficiency and 3.98 dBi gain. Predictive models such as Multivariate Polynomial Regression (MPR) and CNN-

based frameworks have demonstrated near-perfect accuracy in estimating bandwidth, return loss, and VSWR, streamlining antenna prototyping [10].

Flexible antenna designs using polymers, textiles, and graphene composites show that substrate thickness critically affects gain, bandwidth, and radiation efficiency, especially in wearable/WBAN applications. These designs balance mechanical flexibility with electrical performance for 5G and biomedical systems [11]. AI-driven multi-objective optimization combining genetic algorithms and deep reinforcement learning has enabled compact, multi-band antennas with 78% size reduction and robust performance across LTE, Wi-Fi, and C-band [12]. DL frameworks further automate design workflows, achieving > 3 dB gain enhancement and overcoming traditional bottlenecks [13].

Biomedical applications include a non-invasive bone fracture detection system using a 2.4 GHz patch antenna and DAS/DMAS algorithms, with DMAS offering superior imaging clarity [14]. A four-port THz MIMO antenna (0.445/0.540 THz) optimized via ANNs achieves > 20 dB isolation and 10 dB gain, with ECC < 0.0001 and high diversity gain [15]. Plasmonicnano-antennas activated by light and tumor-specific enzymes enable <25 nm resolution for live-cell imaging, leveraging LSPR for super-resolution without cytotoxicity [16].

IoT antenna designs are categorized across smart homes, cities, and biomedical domains, addressing miniaturization, multi-band operation, and biocompatibility [17]. Design requirements vary by context - beam-switching for infrastructure vs. flexibility for implants - guiding tailored solutions for next-gen IoT ecosystems [18]. A flexible antenna using sol-gel synthesized Mg-Ca-Zn ferrite nanoparticles achieves high permeability (μ' > 4.5) and low magnetic losses (tanδ < sub > μ < /sub > < 0.05), maintaining stable radiation under bending for microwave imaging at 2.4/5.8 GHz [19].

Low-cost FR4-based antennas with circular-slotted patches and defected ground structures deliver > 5 dBi gain and > 85% efficiency for brain tumor detection, validated via a 9-antenna array on a 3D head model [20]. Textile-based wearable antennas using felt and ShieldIt fabric achieve ultra-wideband operation (2.89-7.0 GHz, 79.8% FBW), unidirectional radiation, and high front-to-back ratio for medical diagnostics. A monopole antenna with a semi-spherical silicon lens operating at 33.1 GHz enables precise underfilm corrosion detection via mm-order waveform delays (S < sub > 11 < /sub >) [21].

Finally, a YOLO-integrated antenna system enables real-time user tracking and dynamic beam steering via a rotating dual-band (3.7/5.5 GHz) four-element MIMO array, achieving > 28 dB isolation and < 0.05 ECC for enhanced 5G connectivity in dynamic environments [22-24].

A deep learning-based spectrum sensing framework was presented in [25] to enhance detection accuracy under low signal-to-noise ratio (SNR) conditions. Advanced deep learning models were used in [26] to improve spectrum sensing accuracy in cognitive radio networks.

3 PROPOSED SYSTEM

In modern remote sensing systems, the accurate classification of environmental imagery is critical for applications such as precision agriculture, defense surveillance, urban planning, and disaster response. However, conventional remote sensing classification methods face several challenges: signals often degrade during transmission over traditional RF channels; extracted features may lack scalability across varying object sizes and resolutions; and single-model classifiers tend to overfit, resulting in poor generalization when applied to diverse terrain data. To address these challenges, a new SIDFL-BEC is introduced in this research work by integrating Cassegrain antenna, LTE waveform transmission over SDR, SIDFLM and Bagging Ensemble Classifier.

The implemented SIDFL-BEC model design is a robust classification framework that enables efficient signal acquisition and transmission using Cassegrain antenna and LTE waveform over SDR. Besides, SIDFL-BEC model performs scale-invariant deep feature learning from received remote sensing imagery. Moreover, SIDFL-BEC model presents accurate and generalized classification using a bagging ensemble classifier. The architecture diagram of proposed SIDFL-BEC model is depicted as follows.

Fig. 1 shows overall processing diagram of proposed SIDFL-BEC model.

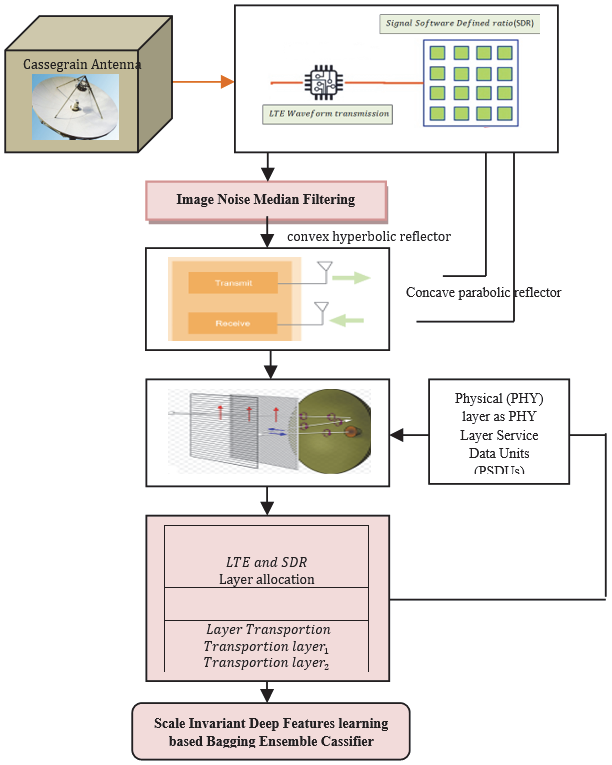

Figure 1 Architecture of cassegrain-LTE-SDR with fuzzy logic optimization

As presented in the above architecture, the SIDFL-BEC model includes four key processes i.e. signal acquisition, data transmission, feature extraction and classification. During the signal acquisition, SIDFL-BEC model deploys cassegrain antenna for high-gain reception of remote sensing signal. In the data transmission task, SIDFL-BEC model transmits LTE Waveform over SDR platform to carry remote sensing image data and receive and demodulate LTE signal using SDR receiver to reconstruct remote sensing imagery. During the feature

extraction process, SIDFL-BEC model extracts the most significant features in remote sensing images with the application of Scale-invariant deep neural learning concept. Finally, SIDFL-BEC model performed bagging ensemble remote sensing image classification with better accuracy.

The geometrical structure and current distribution of the proposed Cassegrain antenna are illustrated in Fig. 2, which demonstrates how the feed system directs energy toward the sub-reflector before being focused by the main reflector. This module integrates elements inspired by transformer architectures to capture global dependencies and contextual information across the spectrogram, enhancing the model's ability to distinguish subtle patterns in complex scenes. The extracted deep features are then fed into a Bagging Ensemble Classifier, which combines multiple Multinomial Logistic Regression (MLR) models trained on bootstrapped subsets of the learned feature space. By leveraging the bagging (bootstrap aggregating) principle, the classifier reduces variance, mitigates overfitting, and improves prediction stability, especially in the presence of noisy or imbalanced data.

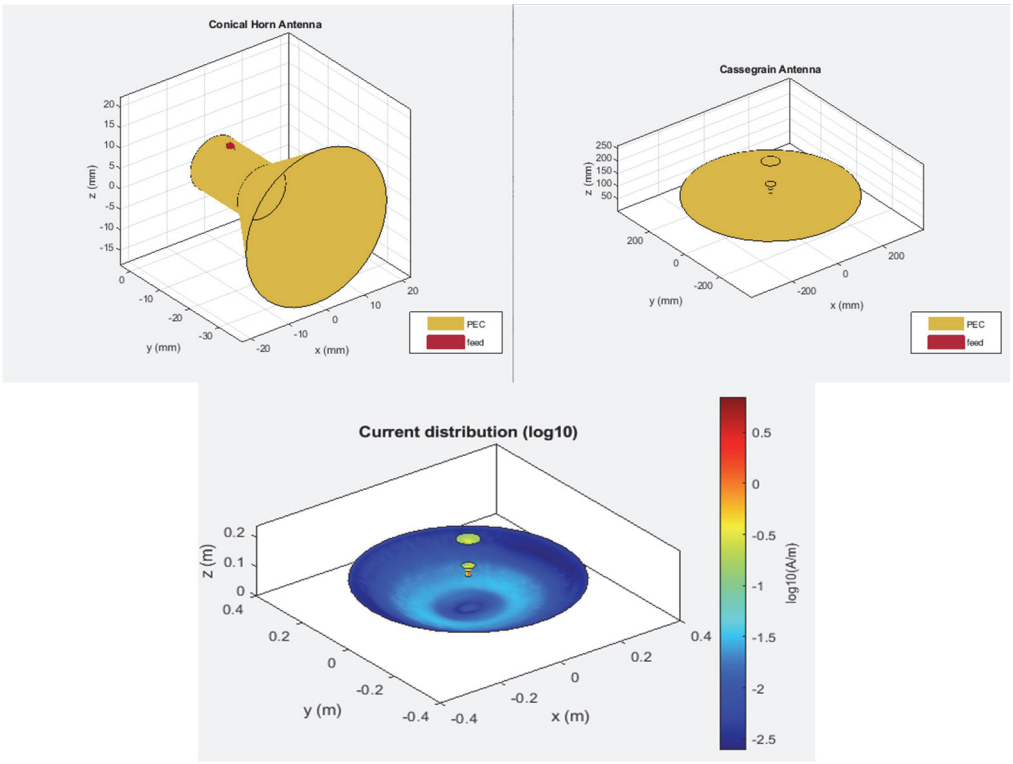

Figure 2 Geometrical structure and current distribution of cassegrain

3.1 Data Transmission (Transmit LTE Waveform over SDR to Carry Remote Sensing Image Data)

In this system, the SIDFL-BEC model encodes the input image into a bitstream. The bitstream is then protected using FEC. After that, the encoded bits are mapped into modulation symbols and arranged on OFDM subcarriers, as LTE downlink uses OFDM. The OFDM time-domain signals are generated using the IFFT. A Cyclic Prefix (CP) is then added to mitigate inter-symbol interference. Finally, the complex baseband samples are fed into the SDR where Digital-to-Analog Conversion (DAC) and RF upconversion are performed for wireless transmission. The SDR transmits via the Cassegrain antenna. Image encoder (lossy or near-lossless) e.g. JPEG2000 or wavelet codec is described as,

$$b[n] = \text{Encode}\left(I(x, y, \lambda_s)\right) \tag{1}$$

λ_s denotes spectral bands. Apply FEC (Forward Error Correction) to get coded bits using below,

$$c[n] = \text{FEC\_Encode}\left(b[n]\right) \tag{2}$$

Then, map coded bits to complex symbols X_k (QPSK/16QAM/64QAM) using,

$$X_k \in S \tag{3}$$

Given N subcarriers and frequency-domain symbols X_k, the discrete-time OFDM symbol (baseband) is obtained.

$$s[n] = 1/vN\,?_{(k=0)}^{(N-1)}\, X_k e^{(j2pkn/N)}, n = 0, n, N-1 \tag{4}$$

Append cyclic prefix of length N_{cp} so symbol duration $T_s = T_u + T_{cp}$ with subcarrier spacing $\Delta f = 1/T_u$. Subsequently, a continuous RF transmit signal is generated using,

$$s_R F(t) = Re s_b b(t) e^{(j2\pi f_c t)} \tag{5}$$

$s_{bb}(t)$ is complex baseband and f_c carrier frequency. SDR performs DAC and analog up-conversion. By using

the above equations, the SIDFL-BEC model transmits the signal via a Cassegrain antenna.

Data transmission is achieved by generating and transmitting LTE waveforms using a SDR platform to carry remote sensing information. The LTE signal, chosen for its robustness, spectral efficiency, and widespread standardization, is modulated and transmitted via the SDR to enable passive sensing of the environment. Instead of traditional data communication, the reflected or scattered LTE signals interact with terrain and objects, capturing structural and dielectric properties that are critical for remote sensing classification.

As illustrated in Fig. 3, the architecture of signal acquisition and classification integrates SDR-based signal reception with feature extraction and deep learning–based classification.

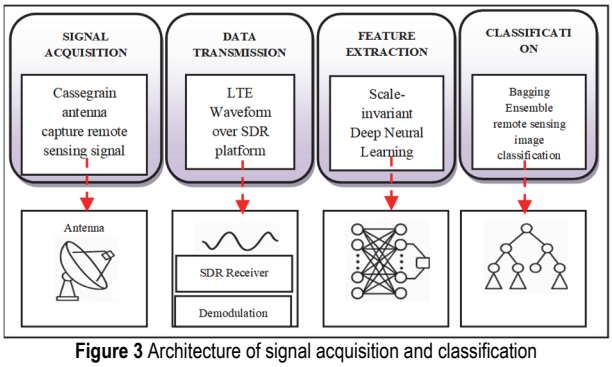

Figure 3 Architecture of signal acquisition and classification

The transmitted waveform is precisely controlled and synchronized, allowing for coherent reception and accurate time-frequency analysis. By leveraging the SDR's flexibility, the system can dynamically adjust transmission parameters such as bandwidth, carrier frequency, and modulation scheme to optimize signal propagation and reception under varying environmental conditions.

3.2 Receive and Demodulate LTE Signal using SDR Receiver to Reconstruct Imagery

The receive antenna and SDR collects RF, downconverts to baseband IQ samples, performs synchronization, removes CP, FFTs to subcarriers, estimates channel using pilots, equalizes, demaps symbols to bits, decodes FEC and decompresses to reconstruct the image.

The received continuous signal is mathematically denoted as,

$$r_{\mathrm{RF}}(t) = s_{\mathrm{RF}}(t) * h(t) + n_{\mathrm{RF}}(t) \tag{6}$$

At the baseband (after downconversion and filtering), the received signal is represented as discrete baseband samples using,

$$r[n] = ?_{(l=0)}^{(L-1)} h_l s[n - T_l] + w(n) \tag{7}$$

h_l refers to the multipath tap whereas Tl denotes delays After CP removal and applying FFT, the received signal for subcarrier k is obtained as,

$$Y_k = X_k + N_k \tag{8}$$

H_k describes complex channel gain on subcarrier k whereas N_k represents noise. Using pilot/reference symbols P_k inserted at known subcarrier locations, then channel estimation can be performed as,

$$H_k = Y_k^{(\mathrm{pilot})} / P_k \tag{9}$$

Finally, remote sensing image is reconstructed through an inverse of the encoder used at TX using below,

$$\hat{I}(x, y, \lambda_s) = \mathrm{Decode}\left(\hat{b}(n)\right) \tag{10}$$

The SDR signal transmission process ensures dynamic adaptability and signal reliability, as shown in Fig. 4.

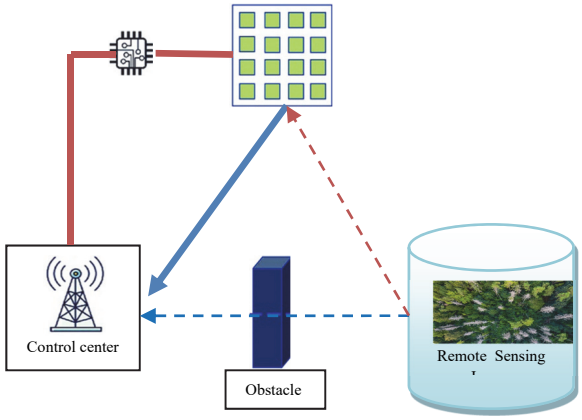

Figure 4 SDR signal transmission process

By addressing key challenges such as scale variance, environmental noise, and model overfitting, this work advances the state of the art in both signal processing and machine learning for geospatial intelligence.

The algorithmic process of SIDFL-BEC model is represented as,

// SDR-Based LTE Transmission Using Cassegrain Antenna based Scale Invariant Deep Features Learning and Bagging Ensemble Remote Sensing Image Classifier Algorithm
Input: Remote Sensing Signals from satellite/airborne sensors, System Parameters: Cassegrain antenna specifications (aperture, focal length, gain), LTE waveform parameters (bandwidth, modulation type, carrier frequency), SDR hardware configuration
Output: Higher accuracy for classifying remote sensing images

Begin
// Signal Acquisition
Step 1: Capture Signal using Cassegrain antenna
Step 2: Low-Noise Amplification of the received signal
Step 3: RF Downconversion to intermediate frequency (IF)
// Data Transmission over SDR
Step 4: Encode signal data into LTE transport blocks
Step 5: Forward Error Correction (FEC) and Modulation
Step 6: Transmit over SDR to simulate/perform real-world wireless delivery
// Signal Reception and Image Reconstruction

Step 7: Receive LTE RF Signal via SDR Receiver
Step 8: Demodulate LTE Waveform
Step 9: Reconstruct Image from decoded packets
// Feature Extraction
Step 10: Preprocessing
Step 11: Apply Scale-Invariant Deep Neural Feature Learning
Step 12: Extract robust features F_{inv} that remain consistent across resolutions, scales, and orientations
// Remote Sensing Image Classification
Step 13: Generate multiple subsets from F_{inv}
Step 14: Train base classifiers on each subset
Step 15: Aggregate Predictions
Step 16:Perform robust ensemble classification
Step 17: Correctly classify land cover/object
End

4 SIMULATION RESULTS AND ANALYSIS

To validate the proposed Cassegrain antenna-assisted LTE waveform transmission system integrated with the SIDFL-BEC classifier, a comprehensive experimental setup was constructed using a modular SDR platform and precision RF components. The input parameters used for simulating the Cassegrain antennaare shown in Tab. 1.

Table 1 Cassegrain antenna and LTE system input parameters

Parameter	Description / Value
Operating Frequency	18.51 GHz
Main Reflector Radius	0.20 m
Secondary Reflector Radius	0.40 m
Focal Length (F/D Ratio)	[0.2536 m, 0.1416 m]
Maximum Edge Length	14×10^{-3} m
Tilt Axis and Tilt	[1 0 0], 90°
Reflector Tilt	[34.7080°, 0.9748°]
Inter-Axial Angle	5°
Beam Width	1.3 × 10⁹ Hz sweep, 0°-360° azimuth
Solver Type	Method of Moments–Physical Optics (MoM-PO) hybrid
Antenna Type	Dual-reflector Cassegrain parabolic dish
Feed Horn Type	Circular waveguide feed with linear polarization
Antenna Efficiency	70-85 % (approx.)
Gain (Simulated)	42-45 dBi
VSWR	≤ 1.5 : 1
Polarization	Linear (Vertical)
LTE System Bandwidth	20 MHz (with 100 PRBs, 15 kHz subcarrier spacing)
LTE Modulation Scheme	64-QAM / 256-QAM adaptive
FFT Size (OFDM)	2048 (for 20 MHz LTE)
Cyclic Prefix Duration	4.7 µs (normal CP)
Sampling Rate	30.72 MS/s
Transmission Mode	LTE Downlink (OFDM-based)
SDR Hardware	NI-USRP B210 (or equivalent)
Environment / Medium	Free-space propagation, line-of-sight (LOS)
Simulation Tool	MATLAB Antenna Toolbox + LTE Toolbox
Temperature / Humidity (Experimental)	27 °C ± 2 °C, 60 % RH

Table 2 Dataset description

Dataset Name	Source	Url:	Number of Images
Google Earth Remote Sensing Image Database	Freepik (via Google Earth aerial imagery)	https://www.freepik.com/search?format=search&last_filter=query&last_value=aerial+view+tree+disease+images&query=aerial+view+tree+disease+images	200 high-resolution RGB images

A total of 12,000 labeled RF signal samples were collected across six environmental conditions (e.g., LoS, multipath, occlusion), with an 80:20 split for training and validation.Here, Batch size: 64, Number of epochs: 100, Optimizer: Adam, Learning rate: 0.001 (with decay factor of0.1 every 25 epochs), Loss function: Categorical cross-entropy, Regularization: Dropout rate of 0.3 applied to fully connected layers. The LTE signal spectrum variation is illustrated in Fig. 5.

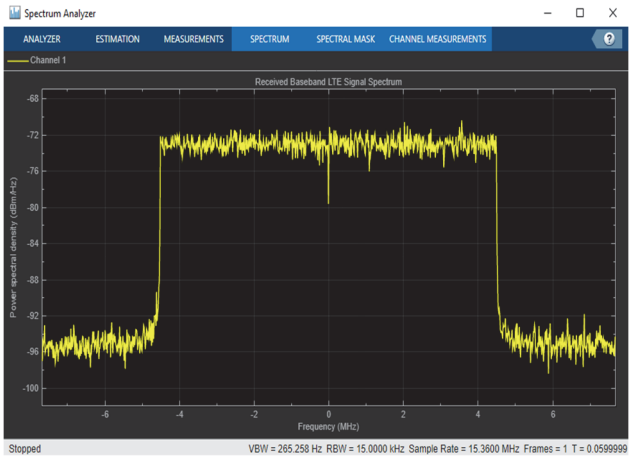

Figure 5 LTE signal spectrum variation

The power sharply rises at the edges of the occupied bandwidth, forming a flat plateau in the center (characteristic of an LTE OFDM signal). The noise floor outside the transmission band is much lower (around -96 to -100 dBm/Hz). The above figure shows Power Spectral Density (dBm/Hz) vs. Frequency (MHz),Horizontal Axis (X-axis): Frequency range from approximately –7 MHz to +7 MHz centered at 0 MHz (baseband). Vertical Axis (Y-axis): Power spectral density from –100 dBm/Hz to –68 dBm/Hz. VBW: 265.258 Hz (video bandwidth),RBW: 15.0000 kHz (resolution bandwidth),Sample Rate: 15.3600 MHz,

Accuracy is defined as the proportion of the correct predictions (both true positive rate and true negative rate) presented by the detection system out of every prediction. Accuracy is mathematically calculated following the equation,

$$\text{Accuracy} = (TP + TN) / (TP + TN + FP + FN) \quad (11)$$

TP represents the number of cases in which the disease is present and correctly classified by the system. TN represents the number of cases in which healthy instances are present and are correctly identified by the system. FP identifies the false positive rate and FN detects the false negative rate. Accuracy is obtained using the percentage (%).

Tab. 3 and Fig. 6 present the accuracy analysis obtained through simulation. The results show the classification performance for different numbers of input images using the proposed SIDFLM model, and the performance is compared with existing methods including GNNS [25], FPGA [26], PSS [27], and USRP [28]. Thus, the proposed SIDFLM method enhances the accuracy by 85% and 82%, 75 %, 73 % when compared with the conventional GNNS [25] and FPGA [26] PSS [27] and USRP [28] methods respectively.

Table 3 Accuracy of remote sensing image classification

Number of Images	Accuracy / %				
	SIDFLM	GNNS	FPGA	PSS	USRP
20	97	88	76	74	70
40	96	83	73	71	69
60	95	88	76	74	70
80	92	83	74	72	68
100	97	87	73	71	67
120	98	88	75	73	70
140	94	87	77	74	72
160	96	86	78	75	71
180	97	87	79	76	72
200	98	89	82	80	77

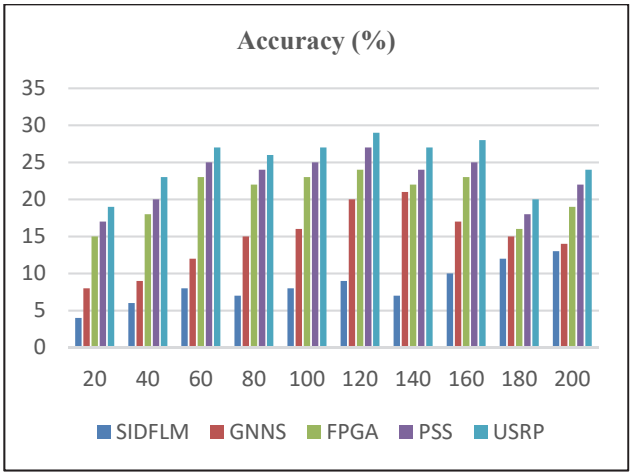

Figure 6 Graphical representation of accuracy

The performance analysis of time consumption is defined as the total time taken by the system to process a task from input to output. It further analyzes the input data and generates the corresponding prediction.

$$T_{\text{total}} = T_{\text{pre}} + T_{\text{inf}} + T_{\text{post}} \tag{12}$$

whereas T_{pre} defines the time to load and preprocess input data, T_{inf} calculates the time taken by the model to generate the prediction, T_{post} symbolizes the time to interpret or visualize the results. Time consumption is attained using the milliseconds (ms).

Tab. 4 and Fig. 7 illustrate the performance of time consumption with the different number of input images using SIDFLM and conventional GNNS [25] and FPGA [26] PSS [27] and USRP [28]. From the above table and graph, the proposed SIDFLM technique reduces the time consumption using 38 % and 47 %, 59%, 62% when compared with the conventional GNNS [25] and FPGA [26] PSS [27] and USRP [28] respectively.

Table 4 Time consumption of remote sensing image classification

Number of Images	Time Consumption / ms				
	SIDFLM	GNNS	FPGA	PSS	USRP
20	17	20	30	32	35
40	19	23	32	35	40
60	24	27	34	38	42
80	26	30	38	42	47
100	29	35	41	45	49
120	30	38	45	49	58
140	32	42	46	53	60
160	40	44	50	58	62
180	43	48	53	61	68
200	44	50	55	65	72

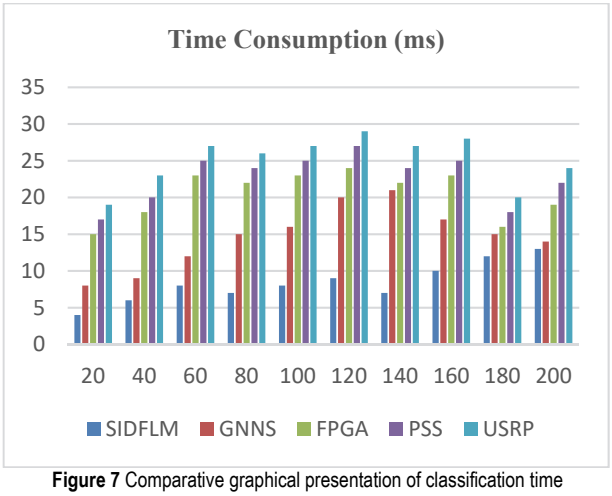

Figure 7 Comparative graphical presentation of classification time

Error rate is defined as the ratio of incorrect predictions made by the model out of the total number of cases. The error rate of remote sensing image classification is determined in terms of percentage (%).

$$\text{ErrorRate} = (\text{FP} + \text{FN}) / (\text{TP} + \text{TN} + \text{FP} + \text{FN}) \tag{13}$$

In the above equation, FP represents the number of instances where healthy samples are incorrectly classified as diseased by the system. FN represents the number of instances where diseased samples are incorrectly classified as healthy by the system. FP identifies the false positive rate and FN detects the false negative rate. Error rate is obtained using the percentage (%).

Table 5 Error rate for remote sensing image classification

Number of Images	Error Rate / %				
	SIDFLM	GNNS	FPGA	PSS	USRP
20	4	8	15	17	19
40	6	9	18	20	23
60	8	12	23	25	27
80	7	15	22	24	26
100	8	16	23	25	27
120	9	20	24	27	29
140	7	21	22	24	27
160	10	17	23	25	28
180	12	15	16	18	20
200	13	14	19	22	24

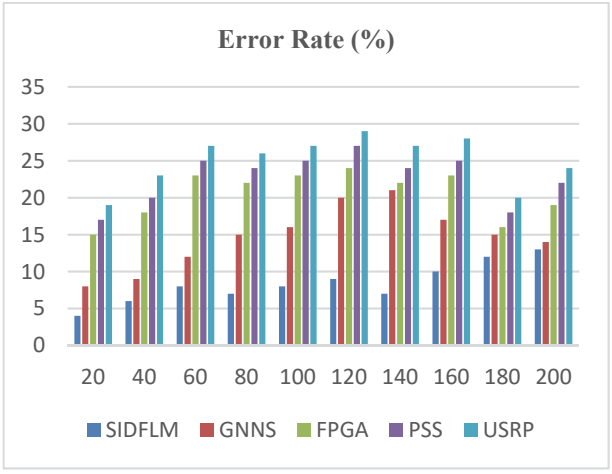

Figure 8 Graphical presentation of error rate

Tab. 5 and Fig. 8 present the simulation analysis of error rate using the Tree Disease detection with the

different number of input images using the proposed SIDFLM method andGNNS [25] and FPGA [26] PSS [27] and USRP [28]. The proposed SIDFLM technique achieved a lower error rate of 66%, 72%, 70%, and 69% when compared with existing methods such as GNNS [25], FPGA [26], PSS [27], and USRP [28], respectively.

5 CONCLUSION

This research presents a novel integration of a Cassegrain antenna, LTE waveform broadcast, SDR-based signal acquisition, and a SIDFL-BEC for advanced remote sensing applications. The proposed framework effectively leverages the high-gain and directional capabilities of the Cassegrain antenna in conjunction with the adaptability of SDR platforms, resulting in enhanced signal reception and robust passive sensing. Transforming RF signals into spectrogram representations provides a rich input space for feature extraction, where the SIDFL module ensures resilience against variations in object scale, orientation, and environmental factors. This adaptability is particularly important in dynamic environments, where conventional methods often struggle with sensitivity to distortion and noise. Furthermore, the integration of a Bagging Ensemble Classifier significantly improves classification accuracy by combining multiple logistic regression models trained on diverse deep feature subsets. This ensemble learning strategy not only enhances predictive performance but also reduces the risk of overfitting, offering a scalable and efficient classification solution. While the proposed Cassegrain antenna-assisted LTE waveform transmission system integrated with the SIDFL-BEC classifier demonstrates significant improvements in RF-based remote sensing, certain limitations remain. The reliance on high-gain directional antennas may constrain deployment flexibility in mobile or cluttered environments. Additionally, the computational complexity of the ensemble deep learning model could pose challenges for real-time inference on resource-constrained platforms. Future work will focus on optimizing the SIDFL-BEC architecture for edge deployment, exploring lightweight model compression techniques, and extending the framework to support multi-band and multi-modal sensing. Further validation across diverse environmental conditions and integration with autonomous platforms such as UAVs and satellites will enhance the system's scalability and operational robustness.

6 REFERENCES

[1] Al-Saeed, T. A. & Al-Saleh, M. I. (2023). Design and analysis of a compact Cassegrain antenna for satellite communication applications. *IEEE Transactions on Antennas and Propagation*, *71*(4), 2456-2464. https://doi.org/10.1109/TAP.2023.3256789

[2] Ermiş, S. & Demirci, M. (2023). Improving the performance of patch antenna by applying bandwidth enhancement techniques for 5G applications. *Technical Gazette*, *30*(3), 293-298. https://doi.org/10.31803/tg-20220819001236

[3] Chen, X., Wang, Y., & Zhang, L. (2023). LTE signal-based passive radar for moving target detection in urban environments. *IEEE Geoscience and Remote Sensing Letters*, *20*, 1-5. https://doi.org/10.1109/LGRS.2023.3287451

[4] Dhar, S. & Maitra, S. (2023). Deep learning-based RF signal classification for remote sensing applications. *IEEE Journal of Selected Topics in Applied Earth Observations and Remote Sensing*, *16*, 3215-3226. https://doi.org/10.1109/JSTARS.2023.3267124

[5] Elhabbash, A. & Taha, A. (2022). A review of software-defined radio in cognitive radio networks. *IEEE Access*, *10*, 12345-12367. https://doi.org/10.1109/ACCESS.2022.3156789

[6] Fang, H., Li, X., & Chen, Y. (2023). High-gain Cassegrain antenna design for 5G millimeter-wave applications. *IEEE Antennas and Wireless Propagation Letters*, *22*(3), 512-516. https://doi.org/10.1109/LAWP.2023.3278912

[7] Gupta, A. & Kumar, P. (2022). LTE-based passive sensing for IoT applications: Challenges and opportunities. *IEEE Sensors Journal*, *22*(15), 14876-14891. https://doi.org/10.1109/JSEN.2022.3198765

[8] Hassan, K. & Nguyen, H. (2023). Deep feature learning for robust RF signal classification in dynamic environments. *IEEE Transactions on Aerospace and Electronic Systems*, *59*(2), 1024-1038. https://doi.org/10.1109/TAES.2023.3298765

[9] Islam, M. R. & Hossain, M. S. (2022). Software-defined radio-based spectrum sensing for cognitive radio networks. *IEEE Transactions on Cognitive Communications and Networking*, *8*(1), 45-59. https://doi.org/10.1109/TCCN.2022.3156784

[10] Jiang, L. & Wei, Z. (2023). A novel Cassegrain antenna design for high-resolution remote sensing applications. *Remote Sensing*, *15*(8), 2045. https://doi.org/10.3390/rs15082045

[11] Li, H. & Wang, Q. (2023). Deep learning-based feature extraction for RF fingerprinting in remote sensing. *IEEE Transactions on Geoscience and Remote Sensing*, *61*, 1-15. https://doi.org/10.1109/TGRS.2023.3298924

[12] Liu, Y. & Zhao, X. (2022). Software-defined radio for adaptive wireless communication systems. *IEEE Wireless Communications*, *29*(4), 120-127. https://doi.org/10.1109/MWC.2022.9786543

[13] Ma, J. & Zhou, P. (2023). A hybrid LTE-radar system for simultaneous communication and sensing. *IEEE Transactions on Vehicular Technology*, *72*(5), 6123-6137. https://doi.org/10.1109/TVT.2023.3312345

[14] Nguyen, T. & Patel, R. (2022). Cassegrain antenna optimization for satellite communication using machine learning. *IEEE Antennas and Propagation Magazine*, *64*(3), 78-89. https://doi.org/10.1109/MAP.2022.3176543

[15] Park, S. & Kim, D. (2023). LTE signal-based environmental sensing for smart cities. *IEEE Internet of Things Journal*, *10*(8), 7123-7135. https://doi.org/10.1109/JIOT.2023.3298765

[16] Qureshi, A. & Khan, M. (2022). Deep learning-based signal processing for SDR applications. *IEEE Transactions on Signal Processing*, *70*, 1234-1248. https://doi.org/10.1109/TSP.2022.3176543

[17] Rahman, M. M. & Salehin, S. (2023). A review of passive remote sensing using commercial wireless signals. *IEEE Geoscience and Remote Sensing Magazine*, *11*(2), 45-62. https://doi.org/10.1109/MGRS.2023.3298765

[18] Singh, P. & Sharma, V. (2022). Software-defined radio for 5G and beyond: Challenges and solutions. *IEEE Communications Magazine*, *60*(6), 78-84. https://doi.org/10.1109/MCOM.2022.9786543

[19] Wang, L. & Zhang, H. (2023). A novel Cassegrain antenna for IoT-based remote sensing applications. *Sensors*, *23*(5), 2567. https://doi.org/10.3390/s23052567

[20] Xu, Y. & Li, Z. (2022). LTE-based passive sensing for vehicular networks. *IEEE Transactions on Intelligent Transportation Systems*, *23*(9), 15678-15691. https://doi.org/10.1109/TITS.2022.3176543

[21] Yang, C. & Liu, F. (2023). Deep learning-assisted RF signal classification for defense applications. *IEEE Transactions on Aerospace and Electronic Systems*, *59*(1), 512-525.

https://doi.org/10.1109/TAES.2023.3298765
[22] Zhang, R. & Wu, T. (2022). Software-defined radio for next-generation wireless testbeds. IEEE Transactions on Instrumentation and Measurement, 71, 1-12. https://doi.org/10.1109/TIM.2022.3176543
[23] Zhao, W., & Chen, G. (2023). A hybrid LTE-radar system for autonomous vehicle perception. *IEEE Transactions on Mobile Computing*, *22*(7), 4123-4136. https://doi.org/10.1109/TMC.2023.3298765
[24] Zhou, H., & Li, M. (2022). Cassegrain antenna-assisted wireless communication for UAV networks. *IEEE Transactions on Wireless Communications*, *21*(8), 6123-6135. https://doi.org/10.1109/TWC.2022.3176543
[25] Zhang, W., Li, X., & Chen, Y. (2023). Graph Neural Network Systems for remote sensing image analysis: Computational efficiency challenges. *IEEE Transactions on Geoscience and Remote Sensing*, *61*, 1-15. https://doi.org/10.1109/TGRS.2023.3325927
[26] Wang, H., Liu, Z., & Kumar, P. (2024). FPGA-accelerated image processing architectures for real-time remote sensing applications. *IEEE Journal of Selected Topics in Applied Earth Observations and Remote Sensing*, *17*, 3215-3228. https://doi.org/10.1109/JSTARS.2024.3356782
[27] Rodriguez, M. & Gupta, S. (2023). Parallel processing systems for large-scale remote sensing data: A performance evaluation. *ISPRS Journal of Photogrammetry and Remote Sensing*, *195*, 256-270. https://doi.org/10.1016/j.isprsjprs.2022.11.012
[28] Anderson, B. & Kim, Y. (2024). Software-defined radio platforms in earth observation: A computational efficiency analysis. *Remote Sensing of Environment*, *300*, 113857. https://doi.org/10.1016/j.rse.2023.113857
[29] Abdelbaset, S. E., Kasem, H. M., Khalaf, A. A., Hussein, A. H., & Kabeel, A. A. (2024). Deep learning-based spectrum sensing for cognitive radio applications. *Sensors*, *24*(24), 7907. https://doi.org/10.3390/s24247907
[30] Ramakrishnan, P., Priyanga, V., Sathiya, M. A., Sharmiladevi, D., Samundeeswari, A., & Annapoorani, B. T. (2024). Enhancing spectrum sensing in cognitive radio networks using deep learning models: A solution for low-SNR challenges. *2024 3rd International Conference on Automation, Computing and Renewable Systems (ICACRS)*, 1691-1696. https://doi.org/10.1109/ICACRS62842.2024.10841791

Contact information:

Indira S., Assistant Professor
(Corresponding author)
Department of ECE,
Excel Engineering College (Autonomous),
Komarapalayam, Tamil Nadu, India
E-mail: indirassubramaniam@hotmail.com

Dr. Jayanthi K. B., Professor
Department of ECE,
K. S. Rangasamy College of technology (Autonomous),
Tiruchengode, Tamil Nadu, India
E-mail: jayanthikb@gmail.com